# Differences in miscible viscous fingering of finite width slices with positive or negative log-mobility ratio

M. Mishra,[1] M. Martin,[2] and A. De Wit[1]

[1]*Nonlinear Physical Chemistry Unit and Center for Nonlinear Phenomena and Complex Systems, Faculté des Sciences, Université Libre de Bruxelles (ULB), CP 231 Campus Plaine, 1050 Brussels, Belgium*

[2]*Ecole Supérieure de Physique et de Chimie Industrielles, Laboratoire de Physique et Mécanique des Milieux Hétérogènes (PMMH, UMR 7636 CNRS, Université Paris 6, Université Paris 7), 10 rue Vauquelin, 75231 Paris Cedex 05, France*

(Received 6 February 2008; published 11 December 2008)

When a sample of fluid of finite size is displaced in a porous medium by another miscible fluid, viscous fingering may occur when the two fluids have different viscosities. Depending whether the sample is more or less viscous than the carrier fluid, the log-mobility ratio $R$ [defined as $R=\ln(\mu_2/\mu_1)$ where $\mu_2$ and $\mu_1$ are the viscosities of the sample and of the carrier] is respectively positive or negative. In the case of a linear displacement of a finite slice of fluid, $R>0$ leads to fingering of the rear interface of the sample where the less viscous carrier invades the more viscous sample. If $R<0$, it is on the contrary the frontal interface of the sample that develops fingers where the less viscous sample displaces the more viscous bulk solution. We investigate here numerically the differences in fingering dynamics between the positive and negative log-mobility ratio cases leading to the growth of fingers against or along the direction of the flow, respectively. To do so, we integrate Darcy's law coupled to a convection-diffusion equation for the concentration of a solute ruling the viscosity of the finite-size sample. The statistical moments of the solute's concentration distribution are analyzed as a function of dimensionless parameters of the problem such as the length of the slice $l$, the log-mobility ratio $R$, and the ratio between transverse and axial dispersion coefficients $\epsilon$. We find that, on average, the mixing zones and the width of the sample broadening due to fingering are larger for negative $R$ than for positive $R$. This is due to the fact that fingers travel quicker in the flow direction than against the flow. Relevance of our results are discussed for interpretation of experimental results obtained in chromatographic separation and for understanding conditions of enhanced spreading of contaminants in aquifers.

DOI: 10.1103/PhysRevE.78.066306 PACS number(s): 47.20.−k, 47.56.+r

## I. INTRODUCTION

When a less viscous fluid of viscosity $\mu_1$ displaces a more viscous one of viscosity $\mu_2>\mu_1$ in a porous medium, the interface between the two fluids becomes unstable and develops fingers. Such a viscous fingering (VF) instability of one interface has been studied extensively in porous media over the last few decades, both experimentally and theoretically (see [1,2] for a review). When only one interface between such two fluids of different mobility is considered, VF occurs when the log-mobility ratio $R$ is positive where $R$ is defined as $R=\ln(\mu_2/\mu_1)$.

Beyond traditional applications in petroleum engineering, viscous fingering has been recognized more recently also to be of possible importance in the spreading of pollution zones in aquifers or in mixing during brine transport in aquifers [3–9] and in band broadening in liquid chromatography used to separate the chemical components of a given sample by passing it through a porous medium [9–23]. The peculiarity of these applications is to deal with a finite width sample of fluid displaced in a porous medium by another bulk fluid. The sample plug can be more viscous or less viscous than the carrier. When a sample of viscous solution is injected into a mobile phase of lower viscosity, the rear interface of the sample band becomes unstable and the frontal interface acts as a stable one. Conversely when a low viscosity sample plug is injected into a higher viscosity mobile phase then the viscous fingers develop at the frontal interface of the sample while the rear interface remains stable.

In chromatography for instance, in the case of polymers or proteins, the viscosity of solutions can strongly vary with concentration. The possible resulting fingering is unpropitious to the separation technique as it contributes to peak broadening and distortions. Such conclusions have been reported by several authors either experimentally [10–17] or numerically [9,16–20]. In aquifer pollution problems, density or viscosity differences between water and localized seawater intrusions, radioactive waste disposal sites, or contaminant plumes can typically enhance spreading between two miscible fluid bodies. This can give rise to enhanced dispersion [4,7] and deformed breakthrough curves [3,6,24].

Miscible viscous fingering of a high viscosity finite width sample displaced by a lower viscous fluid ($R>0$) has been studied numerically quantitatively recently [9,18,20]. It was found that fingering of finite samples is a transient phenomenon contributing nevertheless to increase the variance of the output peaks [9,20]. The dynamics of reverse fingering [18], previously studied by Manickam and Homsy [25] in their simulations of fingering of nonmonotonic viscosity profiles, is found in the finite sample case for $R>0$ due to the fact that the frontal stable zone acts as a barrier preventing the growth of the fingers in the flow direction. From the experimental point of view, Cherrak *et al.* [12] have studied viscosity effects in a methanol-isopropanol system and have discussed the influence of VF on separation through the analysis of the statistical moments of the elution profiles. They have observed a significant loss of separation efficiency due to fingering whenever sample and eluent viscosi-

 

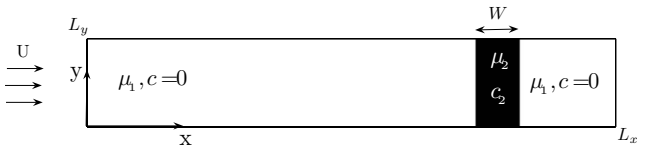


FIG. 1. Sketch of the system.

ties differ by more than 10%. Recently Catchpoole *et al.* [14] have performed experiments to visualize VF in chromatography columns. They have used a mobile phase as well as solute plugs as a mixture of dichloromethane, toluene, and cyclohexanol in a proportion depending on the viscosity required to have sample plugs of viscosity larger or smaller than that of the eluent. This has allowed them to compare fingering of a plug less viscous than the mobile phase, where fingers appear at the forward front, with that of a high viscous solute plug in which the rear front shows the fingering [15]. They concluded that the fingering process observed at the rear front is the negative image of the process of fingering occuring at the forward front.

From these studies, the following question arises: is VF of the frontal or rear interface of a finite-size sample leading to a similar distortion of the output peaks or is there an asymmetry in the dynamics such that one of them would be more detrimental to the widening of the peaks than the other one? In other words, is the fact that, in one case the fingers develop in the direction of the flow while in the other case they grow against it, has an overall influence on the extent of the fingering zone in time?

To obtain insight into these questions, the objective of this particle is to compare the nonlinear dynamics and the averaged properties of miscible VF of finite width slices when the log-mobility ratio $R$ is respectively positive or negative, which leads to VF of the rear or frontal interfaces, respectively. To do so, we have numerically integrated a two-dimensional model of VF coupling Darcy's law to the evolution equation of a solute, the concentration of which rules the viscosity of a finite-size sample. We have compared nonlinear dynamics of the system as well as averaged quantities for both positive and negative $R$ starting from the same initial conditions. We find that VF is more effective in spreading the sample when VF occurs at the frontal interface of a sample rather than at the rear interface. Significant differences on fingering are observed when varying the width $l$ of the slice, the intensity of the log-mobility ratio $R$ or the ratio $\epsilon$ between the transverse and longitudinal dispersion.

The present paper is organized as follows: We first present in Sec. II our model system as well as our numerical integration technique. Section III compares qualitatively the properties of nonlinear fingering of a miscible sample for both positive and negative $R$. Quantitative analysis of these dynamics are made in Sec. IV before a parametric study is conducted in Sec. V. Conclusions are drawn in Sec. VI.

## II. MODEL SYSTEM

Our model system (see Fig. 1) is a two-dimensional porous medium of length $L_x$ and width $L_y$ in which a slice of fluid, hereafter referred to as "the sample," is injected. This sample has a length $W$ and a viscosity $\mu_2$ dependent on the presence of a solute in concentration $c=c_2$. It is displaced by a carrier fluid of viscosity $\mu_1$ initially filling the porous medium and in which the solute concentration is $c=0$. The displacing fluid is injected uniformly with a mean velocity $U$ along the $x$ direction. Following previous works [1,9,20,26–28], the viscosity of the fluids is assumed to be an exponential function of $c$ such that

$$\mu(c) = \mu_1 e^{Rc/c_2}, \tag{1}$$

where the log-mobility ratio $R$ is defined as mentioned previously as $R=\ln \frac{\mu_2}{\mu_1}$. Such an exponential dependence of viscosity on concentration characterizes, to a good approximation, mixtures of a large number of nonassociating liquids as well as of diluted aqueous solutions [29–31]. If $R>0$, then $\mu_2>\mu_1$: the sample is more viscous than the displacing fluid and the rear interface of the sample is unstable towards viscous fingering while the frontal interface is stable and evolves initially only via dispersion. If $R<0$ then $\mu_2<\mu_1$: the sample is less viscous than the carrier fluid, the rear interface is stable while viscous fingering operates at the frontal interface. It is the goal of this paper to compare the nonlinear properties of fingering of finite width slices for $R>0$ and $R<0$.

Assuming the fluid is incompressible and the flow inside the porous medium is governed by Darcy's law, the governing equations for the system are [27,28]

$$\underline{\nabla} \cdot \underline{u} = 0, \tag{2}$$

$$\underline{\nabla} p = -\frac{\mu(c)}{K}\underline{u}, \tag{3}$$

$$\frac{\partial c}{\partial t} + \underline{u} \cdot \underline{\nabla} c = D_x \frac{\partial^2 c}{\partial x^2} + D_y \frac{\partial^2 c}{\partial y^2}, \tag{4}$$

where $K$ is the permeability of the porous medium, $p$ is the pressure, $\underline{u}=(u,v)$ is the two-dimensional velocity field. $D_x$ and $D_y$ are the macroscopic dispersion coefficients of the porous medium along the $x$ and $y$ directions, respectively [20,32–35].

We then nondimensionalize the governing equations by using $U$ as the characteristic velocity, $L_c=D_x/U$ as the length scale, and $t_c=D_x/U^2$ as the time scale. Switching to a frame moving with speed $U$, the governing equations (2)–(4) with the concentration-dependent viscosity equation (1) become [27]

$$\underline{\nabla} \cdot \underline{u} = 0, \tag{5}$$

$$\underline{\nabla} p = -\mu(c)(\underline{u} + \underline{e}_x), \tag{6}$$

$$\frac{\partial c}{\partial t} + \underline{u} \cdot \underline{\nabla} c = \frac{\partial^2 c}{\partial x^2} + \epsilon \frac{\partial^2 c}{\partial y^2}, \tag{7}$$

$$\mu(c) = e^{Rc}, \tag{8}$$

where $\underline{e}_x$ is the unit vector along the $x$ direction, $\epsilon = D_y/D_x$, and the variables denote now dimensionless quantities. Physically, the anisotropic dispersion arises from the fact that the flow, which strongly influences the dispersion process, is not isotropic [32–35]. Here we take $\epsilon$ as a constant in the simulations, except for the specific investigation of its influence in Fig. 15. More general velocity dependent anisotropic dispersion coefficients have been used in other studies of viscous fingering [26,36,37].

Introducing the stream function $\psi(x,y)$, such that $u = \partial\psi/\partial y$ and $v = -\partial\psi/\partial x$, and following Tan and Homsy [28], the momentum and concentration equations (5)–(7) become

$$\nabla^2\psi = -R\left(\frac{\partial\psi}{\partial x}\frac{\partial c}{\partial x} + \frac{\partial\psi}{\partial y}\frac{\partial c}{\partial y} + \frac{\partial c}{\partial y}\right), \tag{9}$$

$$\frac{\partial c}{\partial t} + \frac{\partial\psi}{\partial y}\frac{\partial c}{\partial x} - \frac{\partial\psi}{\partial x}\frac{\partial c}{\partial y} = \frac{\partial^2 c}{\partial x^2} + \epsilon\frac{\partial^2 c}{\partial y^2}, \tag{10}$$

where Eq. (9) has been obtained by eliminating the pressure gradient taking the curl of Darcy's law.

Equations (9) and (10) are numerically solved using the pseudospectral method introduced by Tan and Homsy [28] and successfully adapted in various fingering studies [9,38,39]. The boundary conditions are periodic in both $x$ and $y$ directions. The nondimensional domain is of size $l_y \times l_x$, where $l_y = UL_y/D_x$ and $l_x = UL_x/D_x$. Furthermore $l = UW/D_x$ is the dimensionless length of the sample. For chromatographic columns and aquifers, $l_x$ and $l_y$ can vary in a relative wide range depending on flow velocity, packing particle diameter and system's geometry as discussed in [9,20]. Typical values are here taken as $l_y = 512$ and $l_x = 4096$. The initial condition corresponds to a convectionless fluid embedding a rectangular sample of concentration $c=1$ of size $l_y \times l$ in a $c=0$ background. The middle of the sample is initially located at $x = 4l_x/5$ and $x = l_x/5$ for $R>0$ and $R<0$, respectively. For the numerical simulations, the initial condition corresponds to two back-to-back step functions between $c=0$ and $c=1$ with an intermediate point where $c = 1/2 + Ar$ on the rear front and $c = 1/2 - Ar$ on the frontal one. Here $r$ is a random number between 0 and 1 and $A$ is the amplitude of the noise of order $10^{-3}$. This noise is necessary to trigger the fingering instability on a reasonable computing time. The larger the noise intensity $A$, for example $A$ of order $10^{-1}$ rather than $10^{-3}$, the quicker the onset of the instability [9]. In other words, the curves presented in different figures of Secs. III and IV with time in abscissa can be shifted by a constant time on the left for larger noise intensity. It is necessary to seed the leading front with $(1-c)$ if the rear front is seeded with an initial condition $c$ if we want to ensure that the triggered fingered pattern is the same on the leading front for $R<0$ than the one which develops on the rear front for $R>0$. This will allow us to compare how fingers initiated out of the same noise develop respectively when they grow along the direction of the flow ($R<0$) or against it ($R>0$). In the present simulation spatial discretization step $dx=4$, $dy=4$ is considered. Convergence studies of the numerical method shows that the fingering dynamics is not affected when using smaller time and space steps.

## III. VISCOUS FINGERING WITH POSITIVE AND NEGATIVE $R$

The purpose of our study is to compare the properties of VF of the frontal ($R<0$) and rear interface ($R>0$) of a sample for the same viscosity ratio between the sample and the displacing fluid. To visualize the difference between both cases, fingering dynamics of such finite samples are shown on Fig. 2 for $R=+3$ and $R=-3$, respectively. The evolution is shown in a frame of reference moving with the nondimensional constant speed of the unperturbed sample. Black and white correspond to concentrations $c=1$ and $c=0$, respectively. In the case of a positive log-mobility ratio [$R>0$, Fig. 2(a)] the rear interface of the sample (where the less viscous white bulk fluid displaces the more viscous sample in black) becomes unstable due to the unfavorable viscosity gradient. The other interface at the front where the viscosity gradient is reversed is stable. The opposite occurs (unstable frontal interface and stable rear interface) for the case $R<0$ [Fig. 2(b)]. The fingering dynamics for $R>0$ in the case of finite width samples has already been studied quantitatively numerically in the past [9,18,20].

For both $R>0$ or $<0$, the VF pattern which develops out of the same noise is similar at early times until $t=600$ which can be seen through a visual inspection of Fig. 2 and will be discussed quantitatively in Figs. 3–16. Indeed, until $t=600$, the pattern of the white fingers of the rear interface of Fig. 2(a) is similar to that of the black fingers of the frontal interface of Fig. 2(b). This fingering dynamics is the same as that which would be obtained until this time in the classical VF of one single unstable interface between two semi-infinite regions [28]. Fingers carrying the less viscous fluid move in the downstream direction while reverse fingers carrying more viscous fluid move in the upstream direction of the flow. We define them as forward and backward fingers, respectively. After $t=600$, the specificities related to the fact that we deal here with a finite-size sample come into play: fingers meet the stable interface and the dynamics ceases to be that of one single interface. The two interfaces (one unstable and one stable with regard to VF) start to interact. In the case $R>0$, the stable frontal zone acts as a barrier preventing the forward fingers to further propagate downstream and forces them to reverse their orientation backward once the two fronts start to interact [18]. This kind of reverse displacement can be seen in Fig. 2(a) after $t=600$. For $R<0$ the stable zone at the rear interface acts as a barrier for backward fingers to propagate further in the direction reverse to the flow favoring then the dynamical growth of forward fingers, as seen in Fig. 2(b) after $t=600$. The mixing in the sample enhances during this transition stage due to the reorientation of fingers. At later times, dispersion begins to dilute the sample into the bulk which weakens the viscosity gradients and thus the source of the VF instability preventing the growth of further fingering phenomena. VF is thus a transient phenomenon in the case of finite samples on the contrary to the case of one single interface.

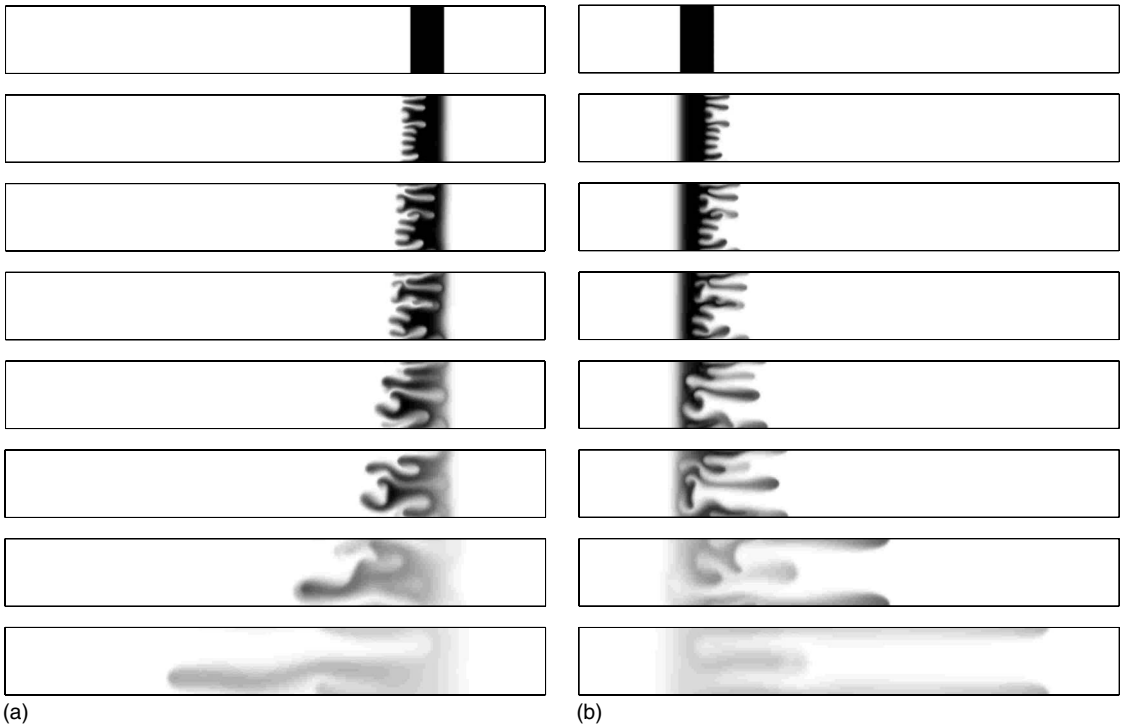


FIG. 2. Density plots of concentration at successive dimensionless times in a frame moving at the velocity of the displacing fluid with $l_y=512$, $l_x=4096$, $l=256$, $\epsilon=1$ for a log-mobility ratio (a) $R=3$ and (b) $R=-3$. From top to bottom: $t=0$, 400, 500, 600, 800, 1000, 2000, and 4000.

Let us focus now on the differences between backward and forward fingers. Reverse fingering has been discussed by Manickam and Homsy [25] in the context of nonmonotonic viscosity profiles and their results for strong frontal stable zones are similar to our findings for VF of a finite sample when $R>0$. A visual comparison of Figs. 2(a) and 2(b) at later times reveals that forward fingers have stretched farther to the right for $R<0$ than backward fingers to the left for $R>0$, while the initial condition was the same for both simulations. This shows on this specific example that VF of a finite-size sample with positive $R$ is eventually not exactly analogous to the one obtained when $R<0$. To further discuss these differences, we will now turn to a quantitative analysis of the simulations shown in Fig. 2 before tackling statistical averages on several simulations.

## IV. QUANTITATIVE ANALYSIS

In order to compare the results for both positive and negative $R$ quantitatively, we introduce several quantities useful to characterize the properties of fingers [26,28].

### A. Transversely averaged profiles

Transversely averaged profiles of concentration are a classical measure done in experimental [3,24] and theoretical studies of VF [9,20,26,28] and allow to gain insight into properties of the dynamics averaged on the cross section of the reactor. They are defined as

$$\bar{c}(x,t) = \frac{1}{l_y}\int_0^{l_y} c(x,y,t)dy \tag{11}$$

and can be related to typical information measured by detectors placed along a chromatographic column for instance [24]. Figure 3 depicts $\bar{c}(x,t)$ at successive times for the simulations presented in Fig. 2. The deformation with bumps at the rear interface (frontal interface) for $R=3$ ($R=-3$) witnesses the presence of fingering at the unstable interface. On the contrary, the frontal (rear) interface for $R>0$ ($R<0$) shows at early time the standard error function characterizing the simple dispersion of a stable front. After a while, both fronts start to interact, a feature specific to VF of finite slices. It is then observed that, as a consequence of dispersion and fingering of the sample, the maximum of $\bar{c}(x,t)$ ceases to be equal to one. We arbitrarily define the time at which the two fronts start to interact as the time for which this constant concentration plateau $c=1$ ceases to exist. It can be seen from Figs. 3(a) and 3(b) that the constant concentration plateau of $c=1$ stays longer for negative $R$, i.e., the interaction between the two interfaces occurs at a later time for $R<0$ than for $R>0$ for a same magnitude of $R$.

### B. Interfacial length

The time at which the rear and frontal interfaces meet can be measured very accurately from another interesting quantity which is the interface length $I$ of the deformed interfaces defined as [40]

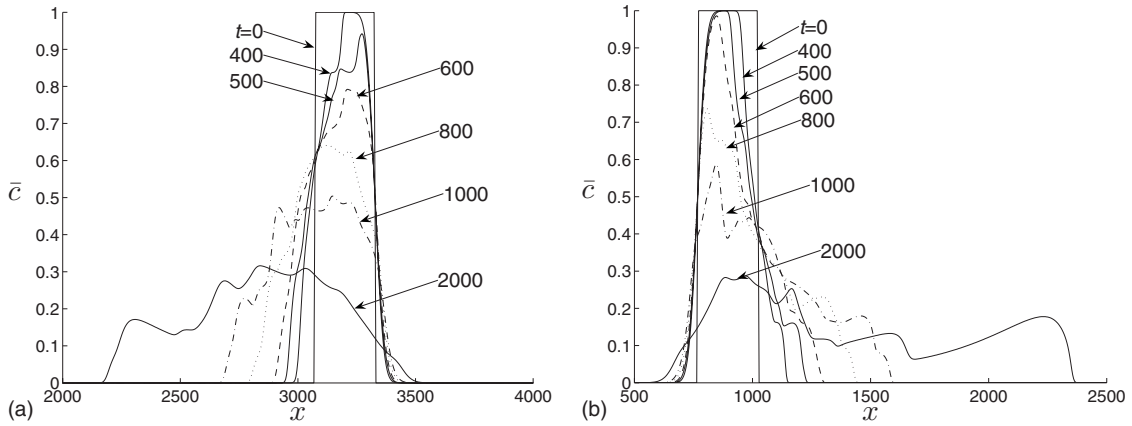


FIG. 3. Transversely averaged concentration profiles $\bar{c}(x,t)$ corresponding to the simulations of Fig. 2 at successive times $t=0$, 400, 500, 600, 800, 1000, and 2000. (a) $R=3$, unstable rear interface with stable frontal interface and (b) $R=-3$, unstable frontal interface with stable rear interface.

$$I(t) = \int_0^{l_y} \int_0^{l_x} \left[ \left( \frac{\partial c}{\partial x} \right)^2 + \left( \frac{\partial c}{\partial y} \right)^2 \right]^{1/2} dxdy. \qquad (12)$$

This quantity is a measurement of the temporal variation of the axial and transverse gradients of concentration. The interfacial length $I$ is plotted as a function of time in Fig. 4 for the simulations shown in Fig. 2. The length $I$ remains constant in the initial diffusive regime then grows strongly with the onset of viscous fingers.

For a pure diffusive displacement along $x$ ($R=0$, $\partial c/\partial y=0$), the base state profile corresponds to two back-to-back error functions separated by a distance $l$ which start to interact at a time $t=l^2/32$ [20]. The corresponding interfacial length is then a constant value of $2l_y$ as long as the two interfaces of the finite sample do not interact, i.e., as long as $t<l^2/32$. This time depends on the sensitivity level of detecting the deviation of the maximum concentration $\bar{c}_{max}$ close to a difference of 2% from the initial value of 1 and it corresponds to all the values of the normal distribution lying within two standard deviations ($2\sigma$) of the mean. In practice, for a normal distribution, one often consider that the data are within $2\sigma$ of the mean as this accounts for about 96% of the distribution and we observe that our simulation is more appropriate for this assumption. For $l=256$, the onset time of interaction of both interfaces is $l^2/32=2048$ and close after this time a decrease of the interfacial length for $R=0$ is observed (see Fig. 4).

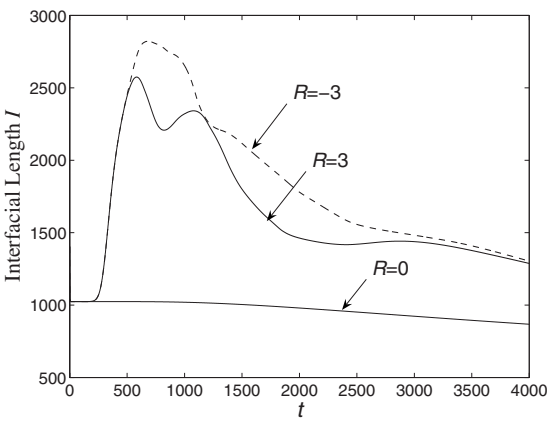


FIG. 4. Temporal evolution of the interfacial length $I$ for the simulations of Fig. 2. $R=3$ (solid line) and $R=-3$ (dashed line). $R=0$ corresponds to the pure dispersion.

On the other hand, it can be seen that the onset time of VF instability at which $I$ departs from its value in the stable case is the same for both $R=3$ and $R=-3$. Then the length $I$ grows exactly the same way at early times for both cases. This is due to the fact that the fingering dynamics gives the same pattern in both cases until roughly $t=600$ (see Fig. 2). Meanwhile, however, when the left and right interfaces touch each other the length $I$ starts decreasing suddenly at roughly $t\sim 500$ for $R=3$ and $t\sim 700$ for $R=-3$. These times correspond to the times when fingers reorient themselves (Fig. 2) and when $\bar{c}_{max}$ becomes lower than 1 (Fig. 3). The measurement of $I(t)$ shows that VF speeds up the meeting of the two interfaces with regard to the pure diffusive case and that this meeting occurs earlier for positive than for negative $R$.

### C. Mixing lengths

The length of the fingering zone, also classically referred to as the "mixing length" in the viscous fingering literature [1], is an important measure in the study of VF quantifying the extent of the zone where the two miscible fluids mix one into the other. In order to quantify the spreading of the forward and backward fingers we define two types of mixing lengths. The forward mixing length $L_d^+$ is defined as the interval between the initial position of the forward interface and $\bar{c}=\delta$ at its right. The backward mixing length $L_d^-$ is taken as the interval between the initial position of the rear interface and $\bar{c}=\delta$ at its left with $\delta=0.01$. These two mixing lengths give insight into the dynamics of forward and backward fingering in a way similar to that used by Manickam and Homsy in their analysis of VF of nonmonotonic profiles [25]. The variations of forward $L_d^+$ and backward $L_d^-$ mixing lengths with time for the simulations of Fig. 2 are presented in Fig. 5(a). Until the onset of VF, these lengths propagate at a diffusive rate such as in the case $R=0$, i.e., $L_d^+$, $L_d^- \propto \sqrt{t}$.

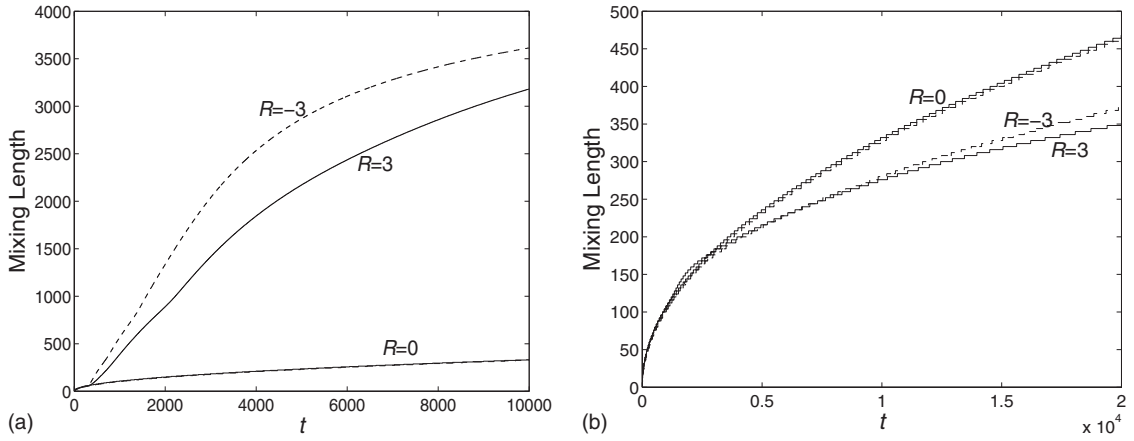


FIG. 5. (a) Mixing length as a function of time at the unstable interfaces for simulations of Fig. 2 for $R=-3$ (dashed line, forward mixing length $L_d^+$) and for $R=3$ (solid line, backward mixing length $L_d^-$), (b) mixing length at the stable interfaces; $R=3$ (dashed line, $L_d^+$) and $R=-3$ (solid line, $L_d^-$). On both graphs, the curve for $R=0$ is the curve of a pure diffusive behavior in which $L_d^+=L_d^-\propto\sqrt{t}$.

When VF sets in, this length then grows faster with a larger slope. It can clearly be seen that the forward fingers at the unstable frontal interface for $R=-3$ travel faster than the backward fingers at the rear interface for $R=3$ as the corresponding mixing length is larger at the same time [Fig. 5(a)]. A similar behavior has been observed by Manickam and Homsy [25] for nonmonotonic viscosity profiles. We note that this phenomenon is here non-negligible as for $t=5000$ for instance, the mixing length is more than 30% larger for $R=-3$ than for $R=3$. This explains why the interaction of both rear and frontal interfaces occurs earlier for $R=3$ than for $R=-3$ as forward fingers take less time to reach the frontal interface (for $R=3$) than the backward fingers to reach the rear interface (for $R=-3$).

The mixing length of the dispersive regime at the stable interfaces (leading front for $R>0$ and rear front for $R<0$) varies at a diffusive rate $\sqrt{t}$, until both interfaces of the finite sample interact. After the onset of interaction between the two interfaces it varies with a power-law exponent smaller than $1/2$ [see Fig. 5(b)], with the stable front for $R=3$ traveling slower than the one for $R=-3$. So we find that the dispersive dynamics at the stable interface undergoes a transition from a pure diffusive regime to another diffusive one after the onset of interaction with the viscous fingering taking place at the other unstable interface.

Although the above definitions of the mixing lengths may lead to multivalued quantities, it is not so for the simulations shown in Fig. 5, even at the largest times.

### D. Statistical moments

In order to further quantify viscous fingering effects for both larger and lower viscosity samples we next compute the first three statistical moments of the transversely averaged concentration distributions $\bar{c}(x,t)$ using the definitions of central normalized moments [9]. The first moment

$$m(t)=\int_0^{l_x} xf(x,t)dx \tag{13}$$

is the center of mass of the distribution, where $f(x,t)=\frac{\bar{c}(x,t)}{\int_0^{l_x}\bar{c}(x,t)dx}$ is the probability density function of the continuous distribution $\bar{c}(x,t)$. With the development of fingers the center of gravity of the sample is displaced towards the back with respect to its initial position for high viscous samples ($R>0$) and the reverse happens, i.e., the center of gravity is displaced towards the right for less viscous samples ($R<0$). The modulus of the first moment of the distributions shown in Fig. 3 is plotted as a function of time in Fig. 6(a) to compare the speed of the displacements for both $R=3$ and $R=-3$. The center of gravity for $R=3$ moves at the same speed as for $R=-3$ until the forward fingers meet the stable front [near $t=600$ see Fig. 6(b), enlarged graph of Fig. 6(a)] when it then migrates slower for $R=3$. This observation of a center of gravity migrating slower (away from the initial position in the moving frame of reference) for more viscous samples than for less viscous ones has already been pointed out by Cherrak *et al.* [12]. For a while, between $t\sim600$ and $t\sim5000$, forward fingers growing in the flow direction (for $R=-3$) do it faster than backward fingers growing upstream (for $R=3$). This faster growth is accompanied by a quicker dilution of the sample which reduces the strength of the VF process and may explain that the asymptotic dispersion-dominated regime, where both kinds of fingers move again at the same speed, is reached quicker for $R=-3$ than for $R=3$.

Figure 6(c) shows the temporal evolution of the variance (second moment of the distribution), defined as

$$\sigma^2(t)=\frac{\int_0^{l_x}\bar{c}(x,t)[x-m(t)]^2dx}{\int_0^{l_x}\bar{c}(x,t)dx}. \tag{14}$$

This quantity gives information on the width of the distribution. It is seen on Fig. 6(c) that, at a same time, the variance of a less viscous sample can be up to 30% larger than that of a more viscous sample. This is related again to the fact that VF widens more the samples when fingers evolve in the direction of the flow at the frontal interface without encountering any stable barrier ahead. In Fig. 6(d), we eventually plot the absolute value of the skewness $a$ defined as

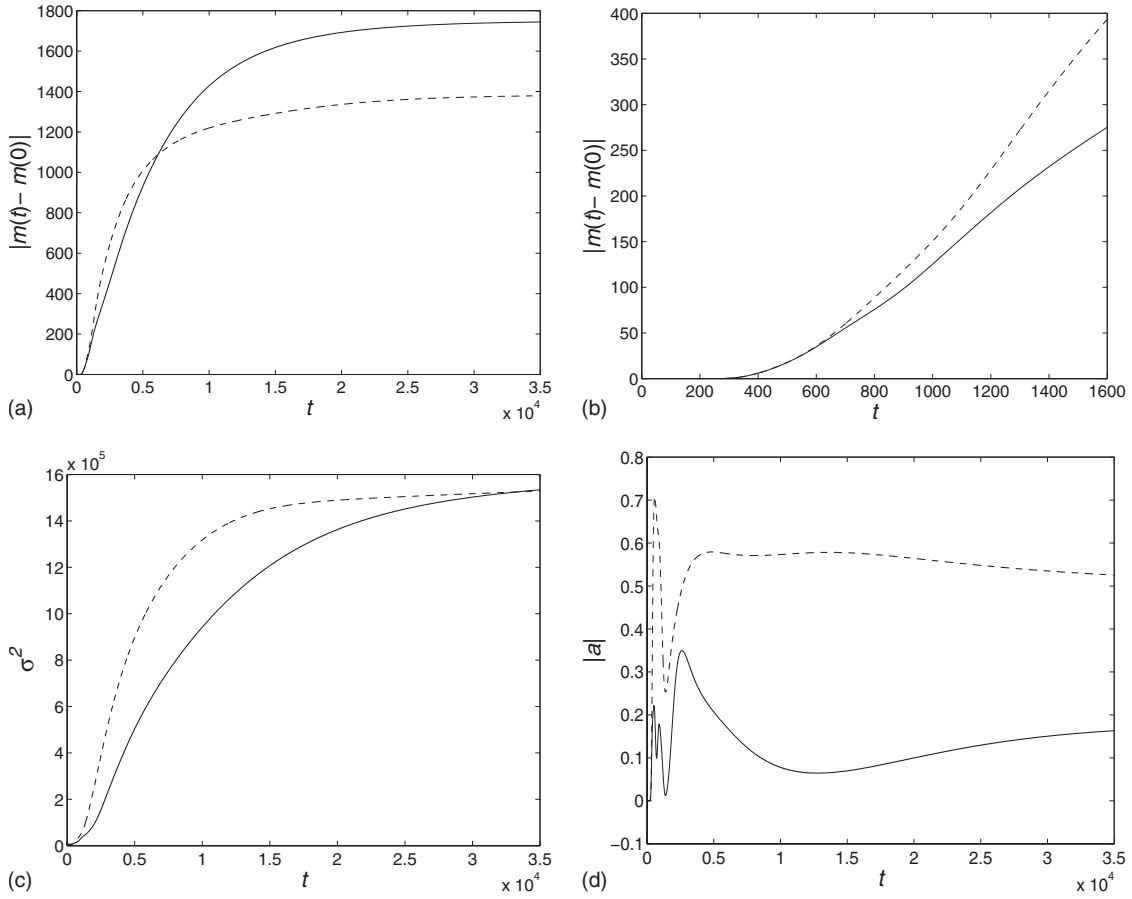


FIG. 6. Temporal changes of the moments of the distribution of $\bar{c}(x,t)$ shown in Fig. 3: (a) Absolute value of the mean position $m$ of the center of mass, (b) enlarged figure (a) showing the initial evolution of $|m(t)-m(0)|$, (c) variance $\sigma^2$ and (d) skewness $a$. Dashed lines ($R=-3$) and solid lines ($R=3$) with $l_y=512$, $l=256$, $\epsilon=1$.

$$a(t) = \frac{\int_0^l \bar{c}(x,t)[x-m(t)]^3 dx / \int_0^l \bar{c}(x,t) dx}{\sigma^3}. \qquad (15)$$

It shows that the mass of the distribution is displaced more to the right for $R=-3$ while mass is rather displaced to the left for $R=3$.

## V. PARAMETER STUDY

### A. Effects of the sample length $l$

The influence of the sample length $l$ on fingering properties for high viscous samples ($R>0$) has already been explained in details previously [9,20]. Peak broadening saturates above a given critical sample length $l_c$ such that the diffusive growth of the asymptotic single finger is reached before the left and right interfaces interact. Let us now compare this phenomenon for both positive and negative log-mobility ratios using the statistical moments of the distribution. To extract the contribution of fingering to peak broadening, we plot on Fig. 7 as a function of time for different finite sample lengths $l$ the quantity $\sigma_f=\sqrt{\sigma^2-\sigma_o^2}$, which is the contribution of viscous fingering to the variance $\sigma^2$. Here $\sigma_o^2=l^2/12+2t$ is the variance of a stable sample ($R=0$), where the first term corresponds to the contribution due to the initial sample width $l$ while the linear term in $t$ corresponds to the contribution of dispersive mixing. We see that the onset of viscous fingering (time at which $\sigma_f$ departs from zero) is the same for both $R=3$ and $-3$, but deformation due to fingering grows faster for less viscous samples ($R<0$). Furthermore, the asymptotic diffusive state (reached here when $\sigma_f$ becomes constant) is reached quicker for $R=-3$ than for $R=3$. For a small sample length $l=256$, the

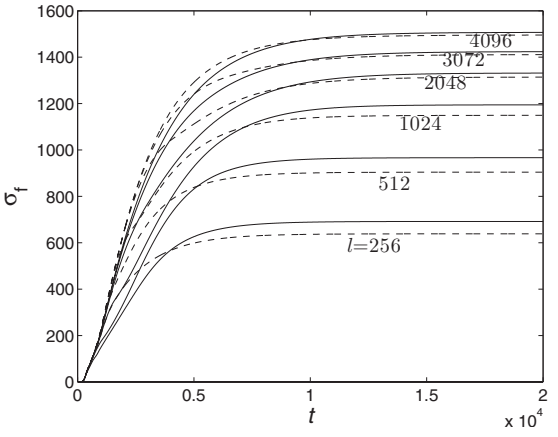


FIG. 7. Effects of the sample length $l$ on $\sigma_f$ for $l_y=256$, $\epsilon=1$; dashed lines ($R=-3$) and solid lines ($R=3$).

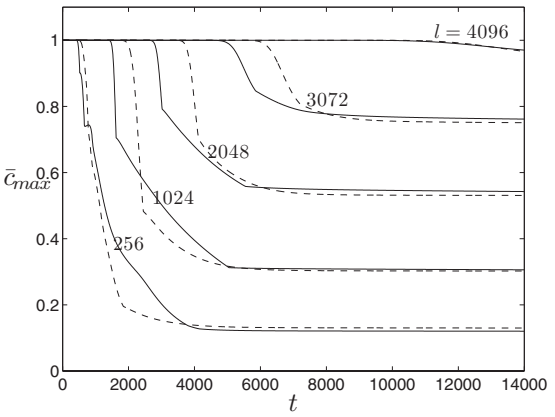


FIG. 8. Effects of the sample length $l$ on the onset time of interaction between left and right fronts of the sample obtained by a measurement of the temporal evolution of $\bar{c}_{\max}$ for $l_y=256$, $\epsilon=1$; dashed lines ($R=-3$) and solid lines ($R=3$).

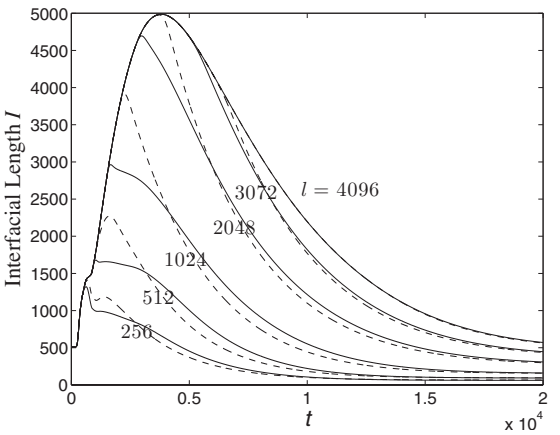


FIG. 10. Effects of the sample length $l$ on the interfacial length for $l_y=256$, $\epsilon=1$. Dashed lines ($R=-3$) and solid lines ($R=3$).

fingering contribution to the variance $\sigma_f$ is larger for $R=3$ than for $R=-3$ in the asymptotic diffusive regime. But this difference reduces for sample lengths $l=512$, 1024 and there is a critical length $l_d \sim 3072$ above which $\sigma_f$ is almost the same for both positive and negative $R$ (see Fig. 7). For $l < l_d$, the time at which the asymptotic diffusive state is reached is larger than the time at which both interfaces of the sample interact and the opposite happens for $l > l_d$. This is observed by comparing the time at which $\bar{c}_{\max}$ deviates from the constant concentration plateau value 1 for different $l$ (Fig. 8) and the asymptotic diffusive time for different $l$ of Fig. 7.

The center of gravity migrates towards the back for $R=3$ and towards the front for $R=-3$ with the same speed for $l=3072$, 4096 different than the speed for smaller length $l=256$, as seen in Fig. 9(a). Hence, we find that fingering does not have any noticeable different effect on the output peak between a positive or negative $R$ of same magnitude for any finite extent of the sample $l > l_d$. The lateral asymmetry of the output peak for positive and negative $R$ is just the symmetric one of the other for any $l > l_d$ in the asymptotic diffusive regime which can be seen in Fig. 9(b), as the absolute value of the skewness is roughly the same for $R=3$ and $-3$ for $l=3072$, 4096 while it differs for $l=128$ in the diffusive regime.

Figure 10 shows the influence of the sample length $l$ on the interfacial length $I$ defined in Eq. (12). The time of reorientation of the forward fingers for $R>0$ and of the backward fingers for $R<0$ is nothing else but the time of the interaction between the rear and frontal interfaces of the sample. This onset time of the interaction of both interfaces at which $I$ starts declining appears later in a longer sample than in a smaller one. This interfacial length also confirms the observation of Fig. 8 that the interaction between both interfaces appears at a later time for a less viscous sample than for a more viscous one for $l < l_d$. But for a sample length $l > l_d$, the interfacial length grows with the same value for both $R=3$ and $-3$ and decays at the same time (see Fig. 10 for $l=4096$). This is due to the emergence of a similar pattern for the fingers as well as because the coarsening of fingers occurs at the same time. In all cases, the fact that $I$ starts declining after a while corresponds to a decrease of the gradient of concentration due either to the interaction between rear and frontal interfaces of the sample (length $l$

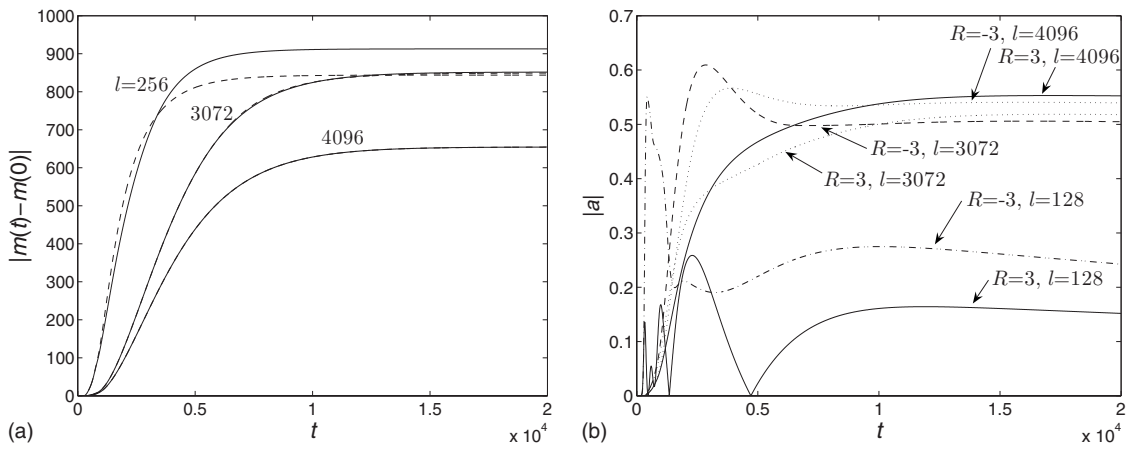


FIG. 9. (a) Effects of the sample length $l$ on the temporal evolution of the center of mass (absolute value of the first moment); dashed lines ($R=-3$) and solid lines ($R=3$). (b) Effect of the sample length $l$ on the absolute value of the skewness for $l_y=256$, $\epsilon=1$, and $R=\pm 3$.

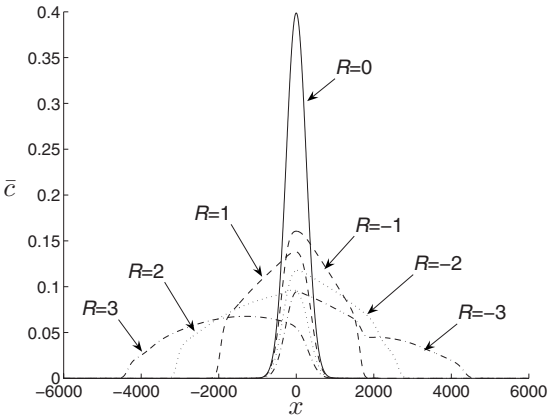


FIG. 11. Transverse average concentration profiles at $t=30\,000$ for $l_y=512$, $l=256$, $\epsilon=1$, and different values of the log-mobility ratio $R$.

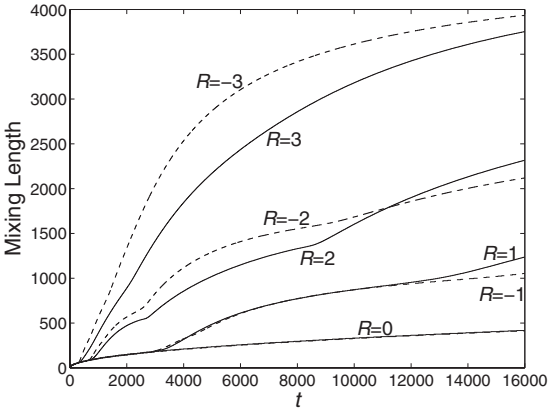


FIG. 13. Influence of the log-mobility ratio $R$ on forward (dashed lines $L_d^+$) and backward (solid lines $L_d^-$) mixing lengths for $l_y=512$, $l=256$, and $\epsilon=1$.

$<l_d$) or because of dispersion taking over before the onset of the interaction between the interfaces ($l>l_d$).

### B. Effect of the log-mobility ratio $R$

The classical effect of $R$ on viscous fingering, i.e., that the systems is more unstable and hence the onset time of viscous fingering decreases with increasing $R$ is well known [1,27]. In order to see the significant effects of $R$ on the viscous fingering of the finite samples for both positive and negative values of $R$ we have plotted $\bar{c}(x,t)$ at a fixed time $t=30\,000$ in Fig. 11 for $l_y=512$, $l=256$, $\epsilon=1$. The initial sample has the same center of mass for all $R$. For the stable case $R=0$ it is a Gaussian displacement. For the sample with $R>0$ the leading front (stable front) originates at the same value as $R=0$ but the deformation is seen at the rear front while the reverse appears for $R<0$. The maximum of the peak is lower for $R>0$ than for $R<0$.

The asymptotic diffusive regime is reached earlier for larger values of $R$ (see Fig. 12) because forward or backward fingers propagate faster for larger values of $R$ than for smaller $R$. This is also seen from Fig. 13 featuring the temporal dependence of $L_d^+$ or $L_d^-$ for different values of $R$. The differences in the growth of the forward and backward mixing lengths in the nonlinear regime reduce when $R$ is decreased. To examine more clearly the symmetry of the peak profile on the basis of the variance of the distribution, we have plotted as a function of $R$ the quantity $\langle\sigma_\infty\rangle$ (see Fig. 14) the averaged value of $\sigma_\infty$ (the value of $\sigma_f$ in the asymptotic diffusion regime [9]) for ten different noise realization simulations. For lower values of $R$, $\langle\sigma_\infty\rangle$ is more symmetric with respect to $R=0$ and for larger $R$ they are more asymmetric.

Such kind of observations enlighten the findings by Cherrak *et al.* [12] [see Figs. 3, 4, and 5(a) of their paper] in their experimental investigation of viscosity effects in the spreading of a sample of mixture of methanol and isopropanol of different viscosities.

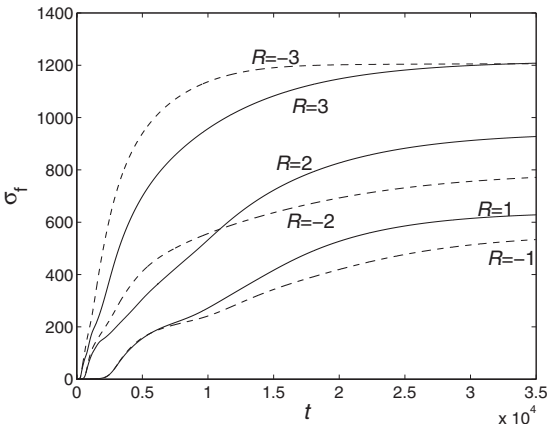


FIG. 12. Temporal evolution of the variance due to fingering $\sigma_f$ for various values of the log-mobility ratio $R$ for $l_y=512$, $l=256$, and $\epsilon=1$.

### C. Effect of the ratio of dispersion coefficients $\epsilon$

Figure 15 shows the influence of the ratio of dispersion coefficients $\epsilon$ on fingering for $l_y=128$, $l=128$, and various log-mobility ratios $R$. It is observed that decreasing $\epsilon$ increases broadening of the peak, as larger $\langle\sigma_\infty\rangle$ are obtained for both negative and positive log-mobility ratios. It is due to

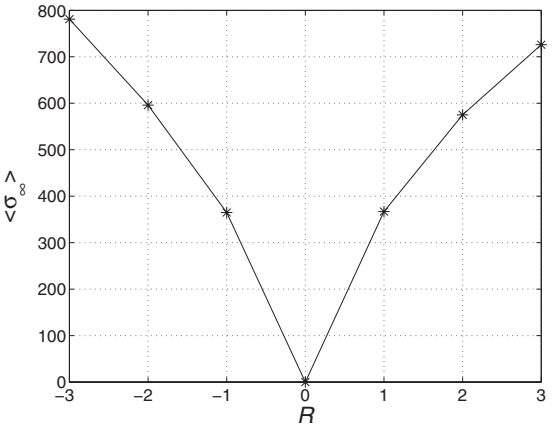


FIG. 14. Influence of the log-mobility ratio $R$ on $\langle\sigma_\infty\rangle$ for $l_y=512$, $l=128$, and $\epsilon=1$.

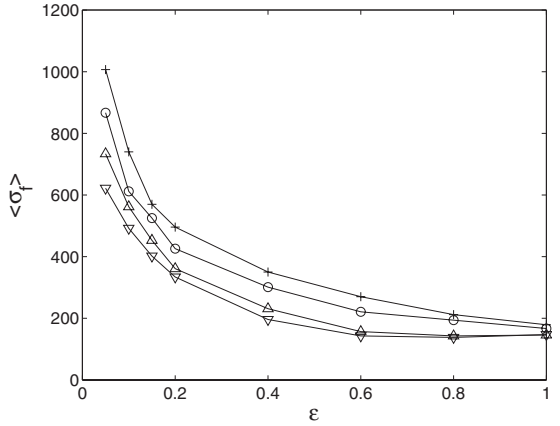


FIG. 15. Influence of the ratio between transverse and longitudinal dispersion coefficients $\epsilon$ on $\langle \sigma_\infty \rangle$ for $l_y=128$, $l=128$, and (+) $R=-3$, (○) $R=3$, (△) $R=-2$, (∇) $R=2$.

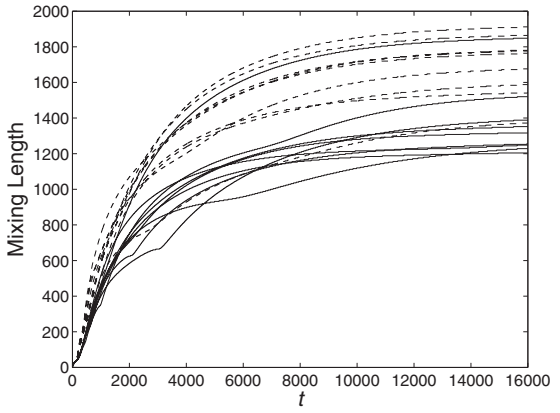


FIG. 16. Mixing lengths as a function of time for $l_y=128$, $l=128$, $\epsilon=0.2$ ($L_d^+$ dashed lines, $R=-3$; $L_d^-$ solid lines, $R=3$) for nine different realizations of the noise seeding the initial condition.

the fact that smaller transverse dispersion assists the growth of the forward fingers more than that of the backward fingers. This is further seen on Fig. 16 in which the mixing lengths $L_d^+$ for $R=-3$ and $L_d^-$ for $R=3$ are plotted for nine different noise realizations of simulations. For chromatography application where $\epsilon$ is expected to be very small, $\epsilon \sim 0.04$, the effects of fingering are hence more vigorous for $R<0$ than for $R>0$.

## VI. CONCLUSION

In the case of one single interface between two semi-infinite miscible fluids of different viscosities with a monotonous viscosity-concentration profile, VF occurs only when a less viscous fluid pushes a more viscous one, i.e., when the log-mobility ratio $R>0$. The situation is different in the case of finite slices of one fluid of given viscosity embedded in the bulk of another displacing fluid. Depending on whether $R$ is positive or negative, it is then, respectively, the rear or frontal interface of the sample that features viscous fingering. We have shown here by numerical simulations of miscible fingering of finite width slices that the properties of fingering for, respectively, positive and negative $R$ can be quite different on average. For one given identical realization of the noise seeding the instability, fingers grow eventually on a longer distance for a given large time when $R<0$ than for $R>0$. The difference can lead up to 30% larger mixing length or variance for $R<0$. This is due to the fact that, for $R<0$, fingers develop at the frontal interface in the direction of the flow, while for $R>0$, fingers grow at the rear of the sample against the flow. Quantitative measurements of transversely averaged profiles, interfacial and mixing lengths, as well as of the statistical moments of the distribution of the sample concentration further show that the influence of VF on the spreading of the sample is more important for $R<0$ than for $R>0$, all other conditions being equal. This shows that VF is more detrimental to chromatographic separation and to spreading of localized pollution zones when the sample is less viscous than the carrier fluid than when it is the displacing fluid which has the larger viscosity.

## ACKNOWLEDGMENTS

A.D.W. and M. Mishra from ULB thank A. Zebib and P. Trevelyan for fruitful discussions and acknowledge financial support from the Communauté française de Belgique (Actions de Recherches Concertées Programme), FNRS, and Prodex. The collaboration between our ULB and ESPCI teams is financially supported by a French (Programme d'actions Intégrés No. 08948YD) - Belgian (CGRI) Tournesol grant.

[1] G. M. Homsy, Annu. Rev. Fluid Mech. **19**, 271 (1987).
[2] K. V. McCloud and J. V. Maher, Phys. Rep. **260**, 139 (1995).
[3] V. Kretz, P. Berest, J. P. Hulin, and D. Salin, Water Resour. Res. **39**, 1032 (2003).
[4] C. Welty, A. C. Kane III, and L. J. Kauffman, Water Resour. Res. **39**, 1150 (2003).
[5] C. Y. Jiao and H. Hotzl, Transp. Porous Media **54**, 125 (2004).
[6] M. Wood, C. T. Simmons, and J. L. Hutson, Water Resour. Res. **40**, W03505 (2004).
[7] R. S. Woumeni and M. Vauclin, Adv. Water Resour. **29**, 1037 (2006).
[8] T. C. Flowers and J. R. Hunt, Water Resour. Res. **43**, W01407 (2007).
[9] A. De Wit, Y. Bertho, and M. Martin, Phys. Fluids **17**, 054114 (2005).
[10] M. Czok, A. Katti, and G. Guiochon, J. Chromatogr. **550**, 705 (1991).
[11] L. D. Plante, P. M. Romano, and E. J. Fernandez, Chem. Eng. Sci. **49**, 229 (1994).
[12] D. Cherrak, E. Guernet, P. Cardot, C. Herrenknecht, and M.

Czok, Chromatographia **46**, 647 (1997).
[13] B. S. Broyles, R. A. Shalliker, D. E. Cherrak, and G. Guiochon, J. Chromatogr., A **822**, 173 (1998).
[14] H. J. Catchpoole, R. A. Shalliker, G. R. Dennis, and G. Guiochon, J. Chromatogr., A **1117**, 137 (2006).
[15] R. A. Shalliker, H. J. Catchpoole, G. R. Dennis, and G. Guiochon, J. Chromatogr., A **1142**, 48 (2007).
[16] T. T. Norton and E. J. Fernandez, Ind. Eng. Chem. Res. **35**, 2460 (1996).
[17] E. J. Fernandez, T. T. Norton, W. C. Jung, and J. G. Tsavalas, Biotechnol. Prog. **12**, 480 (1996).
[18] C.-Y. Chen and S.-W. Wang, Int. J. Numer. Methods Heat Fluid Flow **11**, 761 (2001).
[19] M. L. Dickson, T. T. Norton, and E. J. Fernandez, AIChE J. **43**, 409 (1997).
[20] G. Rousseaux, A. De Wit, and M. Martin, J. Chromatogr., A **1149**, 254 (2007).
[21] C. B. Castells and R. C. Castells, J. Chromatogr., A **805**, 55 (1998).
[22] S. Keunchkarian, M. Reta, L. Romero, and C. Castells, J. Chromatogr., A **1119**, 20 (2006).
[23] K. J. Mayfield, R. A. Shalliker, H. J. Catchpoole, A. P. Sweeney, V. Wong, and G. Guiochon, J. Chromatogr., A **1080**, 124 (2005).
[24] J.-C. Bacri, D. Salin, and R. Woumeni, Phys. Rev. Lett. **67**, 2005 (1991).
[25] O. Manickam and G. M. Homsy, Phys. Fluids **6**, 95 (1994).
[26] W. B. Zimmerman and G. M. Homsy, Phys. Fluids A **4**, 2348 (1992).
[27] C. T. Tan and G. M. Homsy, Phys. Fluids **29**, 3549 (1986).
[28] C. T. Tan and G. M. Homsy, Phys. Fluids **31**, 1330 (1988).
[29] S. Arrhenius, Z. Phys. Chem. **1**, 285 (1887).
[30] M. Martin and G. Guiochon, J. Chromatogr. **151**, 267 (1978).
[31] L. R. Snyder and J. J. Kirkland, *Introduction to Modern Liquid Chromatography*, 2nd ed. (Wiley, New York, 1979), pp. 836–839.
[32] G. Guiochon, A. Felinger, D. G. Shirazi, and A. Katti, *Fundamentals of preparative and nonlinear chromatography* (Elsevier, Amsterdam, 2006).
[33] G. Dagan, *Flow and Transport in Porous Formation* (Springer-Verlag, Berlin, 1989).
[34] J. Bear, *Dynamics of fluids in porous media* (Dover Publication Inc., New York, 1972).
[35] E. L. Cussler, *Diffusion and mass transfer in fluid systems* (Cambridge University Press, Cambridge, 1997).
[36] W. B. Zimmerman and G. M. Homsy, Phys. Fluids A **3**, 1859 (1991).
[37] K. Ghesmat and J. Azaiez, Transp. Porous Media **73**, 297 (2008).
[38] A. De Wit and G. M. Homsy, Phys. Fluids **11**, 949 (1999).
[39] A. De Wit, Phys. Fluids **16**, 163 (2004).
[40] C.-Y. Chen and E. Meiburg, J. Fluid Mech. **371**, 233 (1998).